Hindawi
Mathematical Problems in Engineering
Volume 2020, Article ID 5284906, 13 pages
https://doi.org/10.1155/2020/5284906

Research Article

Effects of Homogeneous and Heterogeneous Chemical Features on Oldroyd-B Fluid Flow between Stretching Disks with Velocity and Temperature Boundary Assumptions

Nargis Khan,[1] Muhammad Sadiq Hashmi,[2] Sami Ullah Khan,[3] Faryal Chaudhry,[4] Iskander Tlili,[5,6] and Mostafa Safdari Shadloo[7]

[1]*Department of Mathematics, The Islamia University of Bahawalpur, Bahawalpur 63100, Pakistan*
[2]*Department of Mathematics, The Government Sadiq College Women University, Bahawalpur 63100, Pakistan*
[3]*Department of Mathematics, COMSATS University Islamabad, Sahiwal 57000, Pakistan*
[4]*Department of Mathematics and Statistics, The University of Lahore, Lahore 54000, Pakistan*
[5]*Department for Management of Science and Technology Development, Ton Duc Thang University, Ho Chi Minh City, Vietnam*
[6]*Faculty of Applied Sciences, Ton Duc Thang University, Ho Chi Minh City, Vietnam*
[7]*CORIA-CNRS (UMR6614), Normandie University, INSA of Rouen, 76000 Rouen, France*

Correspondence should be addressed to Iskander Tlili; iskander.tlili@tdtu.edu.vn

Received 21 December 2019; Revised 10 March 2020; Accepted 16 March 2020; Published 30 April 2020

Guest Editor: Praveen Agarwal

This research endeavors the rheological features of Oldroyd-B fluid configured by infinite stretching disks in presence of velocity and thermal slip features. Additionally, the effects of homogeneous and heterogeneous chemical features are also considered. The transmuted flow equations are analytically solved with help of the homotopy analysis method (HAM). It is observed that the homogeneous chemical reaction parameter enhances the concentration distribution, while the heterogeneous reaction reduces the concentration profile. With implementations of temperature jump conditions, the heat transfer from the surfaces of both disks can be effectively controlled. The impacts of various dimensionless parameters are elaborated through graphs and tables.

1. Introduction

The fluid flow between stretching disks is the main motivation of investigators in recent years due to its leading applications in turbine engines, compression, mechanical components transient loading, semiconductor manufacturing, rotating wafers, injection modeling, power transmission, viscometer, lubrications, radial diffusers, geophysics, biomechanics, geothermal, oceanography, thrust bearings, etc. The usage of microdevices has many practical applications in different scientific areas such as surgery, biotechnology, electronic cooling, microchannels, heat pipes, and pumps. The heat and fluid flow characteristics are different for both microdevices and macroscale counterparts. This difference is constituted by velocity slip and temperature jump. The velocity slip is an important feature to analyze the behavior of microflows because no-slip boundary conditions are not applicable to the fluid flow in microelectro-mechanical-systems (MEMS). Also, no-slip boundary conditions show the impractical behavior for the cases such as corner flow, spreading of liquid on a solid substrate, and extrusion of polymer melts from a capillary tube. Therefore, no-slip boundary condition is replaced by slip boundary condition. Further, in the slip flow regime, temperature jump is significantly used to determine the heat transfer. Because of such applications of slip flow, many interesting contributions have been made by investigators in recent years. For instance, Zheng et al. [1] investigated the stretched flow of viscous fluid in presence of velocity as well as thermal slip features. The peristaltic transport of Carreau fluid through a channel with various flow features with application of velocity slip, temperature, and concentration jump has been inspected by Vajravelu et al. [2]. Khan et al. [3] discussed the double diffusion slip flow of viscous fluid over a vertical plate. Xiao et al. [4] presented a mathematical model for fully developed slip flow in a microtube gas problem. This interesting continuation contains the velocity slip of order two and the assumptions of temperature jump constraints. They claimed an effective change up to 15% in the local Nusselt number at room temperature. Similar slip effects have been performed by Rooholghdos and Roohi [5] for a nanoscale flat plate and a microscale cylinder. Another useful contribution regarding the gas flow associated with thermal slip conditions was examined by Le and Roohi [6]. The peristaltic transport of viscous fluid in an asymmetric channel in presence of velocity and temperature boundary conditions has been discussed by Sinha et al. [7]. El-Aziz and Afify [8] examined the heat transfer characteristics for slip flow of Casson fluid subjected to the induced magnetic field. Khan et al. [9] determined the analytical solution based on the Galerkin technique for an upper convected flow of Maxwell fluid in presence of slip features. Muhammad et al. [10] examined the entropy generation aspects in the flow of nanofluid under the action of the second-order slip. The investigation for fractional Maxwell fluid in presence of slip effects and porous medium was performed by Aman et al. [11].

The fluid flow encountered the heat transportation process conveying a diverse engineering and industrial significance in the metal cooling, petroleum engineering, chemical processing, food industries, thermophysical systems, fiber spinning, manufacturing of metallic sheets, and various nuclear processes. Besides this, the thermal performance of disc-shaped bodies had engaged many scholars because of its practical applications in the era of aeronautical sciences. Many engineering and mechanical processes like thermal power generation and heat transfer to automatic control systems encountered the applications of these phenomena. Due to such recurrent applications, several researchers investigate the flow over or flow between two disks. The initial contribution on this topic was led by Kármán and Uber [12] by considering viscous fluid flow between two infinite disks. This study was further extended by many researchers with different flow features. Hayat et al. [13] studied the heat transfer characteristics based on the Fourier law of conduction in third-grade liquid configured by two porous disks. Turkyilmazoglu [14] simulated the numerical solution of hydromagnetic fluid flow near the stagnation point subject to disk rotation. Heat transfer analysis in the hydromagnetic fluid flow caused by a rotating shrinking disk was also performed numerically by Turkyilmazoglu [15]. Soid et al. [16] applied the numerical technique to observe heat transfer phenomenon in viscous fluid for a radially stretching disk. Yin et al. [17] examined the flow thermal characteristics of nanofluid flow due to a rotating disk. Turkyilmazoglu [18] numerically examined the flow of Newtonian fluid through a vertically moving disk. Hashmi et al. [19] analytically explored the mixed convection flow of Oldroyd-B fluid placed between isothermal stretching disks. The idea of flow over stretching surfaces is extremely useful and involved a large number of practical applications in manufacturing processes [20–23]. The spontaneous idea of flow due to a moving surface was originally advised by Sakiadis [24, 25] which encouraged the investigators to pay attention in this direction. The exact solution for a stretching flow problem was successfully provided by Wang [26]. Another investigation in this direction has been suggested by Fang [27] which conferred the viscous fluid flow induced due to a stretched disk. In another attempt, Fang and Zhang [28] derived an exact solution based on the mathematical formulation of Navier Stokes equations modeled in cylindrical coordinates. In fact, such type of flow between two infinite stretching disks arises due to accelerated stretching velocity. Gorder et al. [29] discussed the axisymmetric flow between two infinite stretching disks. Mohyud-Din and Khan [30] implemented effects of nonlinear thermal radiation in flow of Casson fluid concedes between two stretching disks. Slip flow in presence of thermo-diffusion effects in flow of viscous fluid between stretching disks was suggested by Rashidi and his coworkers [31]. Analytical solution based on the homotopy analysis method for flow of viscous fluid through a stretchable disk has been depicted by Khan et al. [32]. In another investigation, Khan et al. [33] examined the viscous dissipation and joule heating effects on the axisymmetric flow of viscous fluid between stretching disks. Khan et al. [34] studied the entropy generation effects on flow of carbon nanotubes between two rotating and stretching disks. The heat transfer analysis based on Cattaneo–Christov heat flux expressions for the flow of micropolar fluid induced by a nonlinear stretching disk was focused by Doh et al. [35]. Renuka et al. [36] computed an analysis solution for the flow of nanofluid, additionally featuring entropy generation features induced by a stretchable spinning disk.

In the recent decade, the study of combined heat and mass transportation has inspired the scientists to examine various aspects of the simultaneous phenomenon due to its arising applications in the real-world problems like reacting systems, cooling towers, marine engineering, distillation columns, hydrometallurgical industry, crop damage via freezing, and copse of trees. The collaboration amongst homogeneous and heterogeneous responses happening on some catalytic surfaces is correlated with the production and employment of chemical species at diverse rates within the fluid and on the catalytic surfaces. Merkin [37] developed a very useful mathematical model to explore the relationship between a surface-based reaction and homogeneous and heterogeneous reactions. Another useful contribution is from Kameswaran et al. [38] where flow of nanoparticles is immersed in a porous medium with additional features of binary chemical reactions. Rashidi et al. [31] address the effects of homogeneous/heterogeneous on a peristaltic transport in a channel. Hayat et al. [39] implemented the effects of second-order velocity slip to examine the flow of chemical reactive viscous nanofluid induced by a permeable stretching surface.

In this present analysis, our focus is to evaluate the driven transport of Oldroyd-B fluid considered within two infinite stretching disks in presence of homogeneous and heterogeneous reactions. Unlike typical studies, here the idea of second-order velocity slip and temperature jump boundary conditions has been implemented. According to the literature survey, no attempt has been made by researchers for such analysis and is presented for the first time. The present flow problem is utilized in presence of applied magnetic field effects which are useful in the industry of metal-working, chemical reactors, plasma materials, modern metallurgical, oil exploration, and extraction of geothermal energy. The analytical solutions of such transmuted flow equations are determined by employing the homotopy analysis method [40–45]. The accuracy of this method is successfully obtained and expressed in a tabular form. Finally, the important feature effective parameters are graphically underlined and discussed for some velocity, temperature, and concentration profiles with technical relevance.

2. Mathematical Modeling

We consider a two-dimensional flow of Oldroyd-B due to infinite stretching disks. Let flow be axisymmetric and considered fluid be incompressible. The velocity slip and temperature jump are also considered at the walls of stretchable disks. A magnetic field with strength B_0 is imposed in z-direction. The effects of electric and induced magnetic fields are neglected. It is assumed that both lower and upper disks are maintained at temperature T_1 and T_2, respectively. Following Merkin and Chaudhary [46], the mathematical expressions repressing the homogeneous-heterogeneous reactions are expressed as

$$A + 2B \longrightarrow 3B, \quad \text{rate} = k_c \alpha \beta^2. \tag{1}$$

The isothermal, first-order reaction associated with a catalyst surface is represented as

$$A \longrightarrow B, \quad \text{rate} = k_s \alpha, \tag{2}$$

where α and β stand for concentrations of chemical species and A, B, k_c, and k_s denote the rate constants. In the present analysis, both reactions are treated as processes which are isothermal. The analysis is performed by opting a cylindrical coordinate (r, θ, z). All the involved expressions are independent of θ due to axisymmetry. The constitutive partial differential equations for Oldroyd-B fluid in presence of chemical reactions are expressed as

$$\frac{1}{r}\frac{\partial}{\partial r}(ru) + \frac{\partial w}{\partial z} = 0, \tag{3}$$

$$\begin{aligned}
u\frac{\partial u}{\partial r} + w\frac{\partial u}{\partial z} = {} & -\frac{1}{\rho}\frac{\partial \rho}{\partial r} + \nu\left(2\frac{\partial^2 u}{\partial r^2} + \frac{\partial^2 w}{\partial r\,\partial z} + \frac{\partial^2 u}{\partial z^2} + \frac{2}{r}\frac{\partial u}{\partial r} - 2\frac{u}{r^2}\right) - \lambda_1'\left(w^2\frac{\partial^2 u}{\partial z^2} + 2uw\frac{\partial^2 u}{\partial r\,\partial z} + \frac{\partial^2 u}{\partial r^2}\right) \\
& + \nu\lambda_2'\left(\frac{4u^2}{r^3} - \frac{2w}{r^2}\frac{\partial u}{\partial z} - \frac{1}{r}\left(\frac{\partial u}{\partial z}\right)^2 - 2\frac{\partial u}{\partial z}\frac{\partial^2 w}{\partial z^2} + w\frac{\partial^3 u}{\partial z^3} - \frac{2u}{r^2}\frac{\partial u}{\partial r} - \frac{\partial^2 u}{\partial z^2}\frac{\partial u}{\partial r} - 2\left(\frac{\partial u}{\partial r}\right)^2 - \frac{1}{r}\frac{\partial u}{\partial z}\frac{\partial w}{\partial r} + \frac{2w}{r}\frac{\partial^2 u}{\partial r\,\partial z} - \frac{\partial u}{\partial z}\frac{\partial^2 u}{\partial r\,\partial z}\right. \\
& \left. - \frac{\partial u}{\partial r}\frac{\partial^2 w}{\partial r\,\partial z} + u\frac{\partial^3 u}{\partial r\,\partial z^2} + w\frac{\partial^3 w}{\partial r\,\partial z^2} + \frac{2u}{r}\frac{\partial^2 u}{\partial r^2} - 2\frac{\partial u}{\partial r}\frac{\partial^2 u}{\partial r^2} - \frac{\partial u}{\partial z}\frac{\partial^2 w}{\partial r^2} + 2w\frac{\partial^3 u}{\partial r^2\partial z} + u\frac{\partial^3 w}{\partial r^2\partial z} + 2u\frac{\partial^3 u}{\partial r^3}\right) + \frac{\sigma B_0^2}{\rho}\left(-u - \lambda_1' w\frac{\partial u}{\partial z}\right),
\end{aligned} \tag{4}$$

$$\begin{aligned}
u\frac{\partial w}{\partial r} + w\frac{\partial w}{\partial z} = {} & -\frac{1}{\rho}\frac{\partial \rho}{\partial z} + \nu\left(\frac{\partial^2 w}{\partial r^2} + \frac{\partial^2 u}{\partial r\,\partial z} + 2\frac{\partial^2 w}{\partial z^2} + \frac{1}{r}\frac{\partial w}{\partial r} + \frac{1}{r}\frac{\partial u}{\partial r}\right) - \lambda_1'\left(w^2\frac{\partial^2 u}{\partial z^2} + 2uw\frac{\partial^2 u}{\partial r\,\partial z} + u^2\frac{\partial^2 u}{\partial r^2}\right) \\
& + \nu\lambda_2'\left(-\frac{u}{r^2}\frac{\partial u}{\partial z} - \frac{1}{r}\frac{\partial u}{\partial z}\frac{\partial w}{\partial z} + \frac{w}{r}\frac{\partial^2 u}{\partial z^2} - 2\frac{\partial w}{\partial z}\frac{\partial^2 w}{\partial z^2} + 2w\frac{\partial^3 w}{\partial z^3} + \frac{u}{r^2}\frac{\partial w}{\partial r} - \frac{1}{r}\frac{\partial w}{\partial r}\frac{\partial u}{\partial z} - \frac{\partial^2 u}{\partial z^2}\frac{\partial w}{\partial r} - \frac{2}{r}\frac{\partial u}{\partial r}\frac{\partial w}{\partial r} + \frac{u}{r}\frac{\partial^2 u}{\partial r\,\partial z} - \frac{\partial w}{\partial z}\frac{\partial^2 u}{\partial r\,\partial z}\right. \\
& \left. + \frac{w}{r}\frac{\partial^2 w}{\partial r\,\partial z} - \frac{\partial w}{\partial r}\frac{\partial^2 w}{\partial r\,\partial z} + w\frac{\partial^3 w}{\partial r\,\partial z^2} + 2u\frac{\partial^2 w}{\partial r\,\partial z^2} - 2\frac{\partial w}{\partial r}\frac{\partial^2 u}{\partial r^2} + \frac{u}{r}\frac{\partial^2 w}{\partial r^2} - \frac{\partial w}{\partial z}\frac{\partial^3 w}{\partial r^2} + u\frac{\partial^3 u}{\partial r^2\partial z} + w\frac{\partial^3 w}{\partial r^2\partial z} + u\frac{\partial^3 w}{\partial r^3}\right.,
\end{aligned} \tag{5}$$

$$u\frac{\partial T}{\partial r} + w\frac{\partial T}{\partial z} = K\left(\frac{\partial^2 T}{\partial r^2} + \frac{1}{r}\frac{\partial T}{\partial r} + \frac{\partial^2 T}{\partial z^2}\right), \tag{6}$$

$$u\frac{\partial \alpha}{\partial r} + w\frac{\partial \alpha}{\partial z} = D_A\left(\frac{\partial^2 \alpha}{\partial r^2} + \frac{1}{r}\frac{\partial \alpha}{\partial r} + \frac{\partial^2 \alpha}{\partial z^2}\right) - k_c\alpha\beta^2, \tag{7}$$

$$u\frac{\partial \beta}{\partial r} + w\frac{\partial \beta}{\partial z} = D_B\left(\frac{\partial^2 \beta}{\partial r^2} + \frac{1}{r}\frac{\partial \beta}{\partial r} + \frac{\partial^2 \beta}{\partial z^2}\right) + k_c\alpha\beta^2, \tag{8}$$

where u and w are the radial and axial components of velocities, respectively, p is the pressure, ρ is the fluid density, μ stands for dynamic viscosity of fluid, $\nu = (\mu/\rho)$ represents the kinematic viscosity, a and c are the stretching constants, λ_1' is the constant of relaxation, λ_2' is the retardation time, T is the temperature, K is the thermal diffusivity, and D_A, D_B are the diffusion species coefficient of A and B.

2.1. Slip Boundary Conditions. As it has been mentioned earlier that the present flow problem is assisted with slip boundary conditions. For the velocity profile, the derivation of second-order velocity slip is based on the expansion of Taylor series from the first-order Maxwell conditions which are generally expressed as

$$u = u_w + \left(\frac{2-\sigma_u}{\sigma_u}\right)\frac{\partial u}{\partial n}\tau_1 + \left(\frac{2-\sigma_u}{\sigma_u}\right)\tau_1^2\frac{\partial^2 u}{\partial n^2}. \quad (9)$$

For the present analysis, we propose the following second-order boundary conditions:

$$\begin{aligned} u &= ar + \left(\frac{2-\sigma_u}{\sigma_u}\right)\tau_1\frac{\partial u}{\partial z} + \left(\frac{2-\sigma_u}{\sigma_u}\right)\tau_1^2\frac{\partial^2 u}{\partial z^2}, \quad w = 0,\ p = \frac{a\mu\beta_1 r^2}{4d^2}, \text{ at } z = 0, \\ u &= cr - \left(\frac{2-\sigma_u}{\sigma_u}\right)\tau_1\frac{\partial u}{\partial z} - \left(\frac{2-\sigma_u}{\sigma_u}\right)\tau_1^2\frac{\partial^2 u}{\partial z^2}, \quad w = 0,\ p = 0, \text{ at } z = d, \end{aligned} \quad (10)$$

where a and b represent the stretching rates, σ_u is the tangential momentum accommodation coefficient, and τ_1 denotes the molecular mean-free path. It is a well-established fact that the molecular mean-free path is assumed positive, i.e., $\epsilon_1 > 0$ and. $\epsilon_2 < 0$.

2.2. Temperature Jump Boundary Conditions. By using Taylor series second-order expansion for K_n from the first order, Smoluchowski jump condition second-order jump conditions are proposed in [6] as follows:

$$T = T_w + \left(\frac{2-\sigma_T}{\sigma_T}\right)\left(\frac{2\xi}{\xi+1}\right)\frac{1}{\Pr}\tau_2\frac{\partial T}{\partial n} + \left(\frac{2-\sigma_T}{\sigma_T}\right)\left(\frac{2\xi}{\xi+1}\right)\frac{1}{\Pr}\frac{\tau_2^2}{2}\frac{\partial^2 T}{\partial n^2}. \quad (11)$$

The second-order temperature jump boundary conditions associated with the governing equations are

$$\begin{aligned} T &= T_1 + \left(\frac{2-\sigma_T}{\sigma_T}\right)\left(\frac{2\xi}{\xi+1}\right)\frac{1}{\Pr}\tau_2\frac{\partial T}{\partial z} + \left(\frac{2-\sigma_T}{\sigma_T}\right)\left(\frac{2\xi}{\xi+1}\right)\frac{1}{\Pr}\frac{\tau_2^2}{2}\frac{\partial^2 T}{\partial z^2}, \quad \text{at } z = 0, \\ T &= T_2 - \left(\frac{2-\sigma_T}{\sigma_T}\right)\left(\frac{2\xi}{\xi+1}\right)\frac{1}{\Pr}\tau_2\frac{\partial T}{\partial z} + \left(\frac{2-\sigma_T}{\sigma_T}\right)\left(\frac{2\xi}{\xi+1}\right)\frac{1}{\Pr}\frac{\tau_2^2}{2}\frac{\partial^2 T}{\partial z^2}, \quad \text{at } z = d, \end{aligned} \quad (12)$$

where σ_T is the thermal accommodation coefficient and ξ is the specific heat ratio. The other boundary conditions for the flow problem are prescribed by

$$\begin{aligned} &\alpha = \alpha_0 \text{ at } z = 0, \quad D_A\frac{\partial \alpha}{\partial z} = k_s\alpha \text{ at } \quad z = d, \\ &\beta = 0 \text{ at } z = 0, \quad D_B\frac{\partial \beta}{\partial z} = -k_s\alpha \text{ at } \quad z = d. \end{aligned} \quad (13)$$

Introducing the similarity variables,

$$\begin{aligned} u &= -\frac{ar}{2}H'(\eta), \\ w &= a\,dH(\eta), \\ p &= a\mu\left(P(\eta) + \frac{\beta_1 r^2}{4d^2}\right), \\ \eta &= \frac{z}{d}, \\ T &= T_1 + (T_2 - T_1)\theta(\eta), \\ \alpha &= \alpha_0\varphi(\eta), \\ \beta &= \alpha_0 g(\eta), \\ T &= T_1 + (T_2 - T_1)\theta(\eta), \\ \alpha &= \alpha_0\varphi(\eta), \\ \beta &= \alpha_0 g(\eta). \end{aligned} \quad (14)$$

In view of the above similarity variables, equations (4)–(10) yield

$$\frac{R}{2}\left(H'^2 - 2HH''\right) = -\Big[\beta_1 + H''' + \lambda_1' aR\left(HH'H'' - H^2H'''\right) + \lambda_2' a\left(HH^{(iv)} - H''^2\right)\Big] + RM\left(H' + \lambda_1' aHH''\right), \quad (15)$$

$$\theta'' - RPrH\theta' = 0, \quad (16)$$

$$\varphi'' - RSc\left(K_1\varphi g^2 + H\varphi'\right) = 0, \quad (17)$$

$$\delta g'' + RSc\left(K_1\varphi g^2 + Hg'\right) = 0, \quad (18)$$

$$P\prime = \frac{3H''}{2} - RHH' - \lambda_1 RH^2H'', \quad (19)$$

$$\begin{aligned} &H(0) = 0,\\ &H(1) = 0,\\ &H'(0) = -2 + \left(\epsilon_1 H''(0) + \epsilon_2 H'''(0)\right), \end{aligned} \quad (20)$$

$$H'(1) = -2\gamma - \left(\epsilon_1 H''(0) + \epsilon_2 H'''(0)\right), \quad P(0) = 0, \quad (21)$$

$$\begin{aligned} &\theta(0) = \epsilon_3\theta'(0) + \epsilon_4\theta''(0),\\ &\theta(1) = 1 - \left(\epsilon_3\theta'(1) + \epsilon_4\theta''(1)\right), \end{aligned} \quad (22)$$

$$\begin{aligned} \varphi(0) &= 1,\\ \varphi'(1) &= K_2\varphi(1),\\ g(0) &= 0,\\ \delta g'(1) &= -K_2 g(1), \end{aligned} \quad (23)$$

where γ is the wall stretching parameter, R stands for the Reynolds number, Pr is the Prandtl number, ϵ_1 is the first-order velocity slip parameter, M is the Hartmann number, ϵ_2 is the second-order velocity slip parameter, ϵ_3 is the first-order temperature jump parameter, ϵ_4 stands for temperature jump parameter of the second order, Sc represents the Schmidt number, δ is the ratio of the diffusion coefficient, Kn denotes the Knudsen number, K_1 is the strength of the homogeneous reaction, and K_2 is the strength of the heterogeneous reaction and is defined as

$$\begin{aligned} \gamma &= \frac{c}{a},\\ R &= \frac{ad^2}{\nu},\\ \Pr &= \frac{\nu}{\alpha},\\ Kn &= \frac{\tau_{1,2}}{d},\\ \varepsilon_1 &= Kn\left(\frac{2-\sigma_u}{\sigma_u}\right),\\ \varepsilon_2 &= \frac{Kn^2}{2}\left(\frac{2-\sigma_u}{\sigma_u}\right),\\ \varepsilon_3 &= Kn\left(\frac{2-\sigma_T}{\sigma_T}\right)\left(\frac{2\xi}{\xi+1}\right)\frac{1}{\Pr},\\ \varepsilon_4 &= \frac{Kn^2}{2}\left(\frac{2-\sigma_T}{\sigma_T}\right)\left(\frac{2\xi}{\xi+1}\right)\frac{1}{\Pr},\\ \delta &= \frac{D_B}{D_A}. \end{aligned} \quad (24)$$

The constant β_1 has been eliminated from equation (15) as the following procedure:

$$\begin{aligned} H^{(iv)} = {} & RHH''' - \lambda_1 R\left(-HH'H''' - H^2H^{(iv)} + HH''^2 + H'^2H''\right)\\ & - MR\left[H'' + \lambda_1\left(H'H'' + HH'''\right)\right]\\ & - \lambda_2\left(-2H''H''' + H'H^{(iv)} + HH^{(v)}\right), \end{aligned} \quad (25)$$

in which $\lambda_1 = \lambda_1' a$ is the Deborah number for relaxation time and $\lambda_2 = \lambda_2' a$ for the retardation time. It is pointed out here that the diffusion coefficients of chemical species A and B are not equal in general. So, we remarked that constants A and B are of comparable size as a special case and subsequently D_A and D_B are equal, i.e., $\delta = 1$. Equations (16) and (17) lead to the following relation:

$$\begin{aligned} \varphi + g &= 1,\\ \varphi'' - RSc\left(K_1\varphi(1-\varphi)^2 + H\varphi'\right) &= 0,\\ \varphi(0) &= 1,\\ \varphi'(1) &= K_2\varphi(1). \end{aligned} \quad (26)$$

Following mathematical expressions are suggested for the wall skin friction coefficient, local Nusselt number, and local Sherwood number at both surfaces of disks:

$$C_{1f,2f}=\frac{\tau_{rz}\big|_{\eta=0,1}}{(1/2)\rho(\delta r)^2}=2R^{-1}H''(\eta)\big|_{\eta=0,1},$$
$$N_{1u,2u}=-\frac{dk_T(\partial T/\partial z)\big|_{\eta=0,1}}{k_T(T_2-T_1)}=-\theta'(\eta)\big|_{\eta=0,1}, \quad (27)$$
$$Sh=\frac{-(D(\partial C/\partial z))\big|_{\eta=0,1}}{D(C_1-C_2)}=-\varphi'(\eta)\big|_{\eta=0,1}.$$

3. Solution Methodology

To start our simulations, first we introduce the following initial guesses for velocity, temperature, and concentration profiles:

$$\begin{aligned}H_0(\eta)&=\frac{1}{8\epsilon_1+12\epsilon_1^2}(-2\eta(1+\eta)(-1+\eta(1+\gamma)\\&\quad+2\epsilon_1(-2+\eta+\gamma(1+\eta))-6\epsilon_2(1+\eta))),\\\theta_0(\eta)&=\frac{\eta+\epsilon_3}{1+2\epsilon_3},\\\varphi_0(\eta)&=\frac{-1+K_2(1-\eta)}{-1+K_2},\end{aligned} \quad (28)$$

with auxiliary linear operators:

$$L_H=\frac{d^4}{d\eta^4},\quad L_\theta=\frac{d^2}{d\eta^2},\quad L_\varphi=\frac{d^2}{d\eta^2}. \quad (29)$$

The mathematical expressions associated with the zeroth-order deformation problem are defined as

$$\begin{aligned}(1-q)L_H[H(\eta;q)-H_0(\eta)]&=q\hbar_H N_H[H(\eta;q)],\\(1-q)L_\theta[\theta(\eta;q)-\theta_0(\eta)]&=q\hbar_\theta N_\theta[\theta(\eta;q)],\\(1-q)L_\varphi[\varphi(\eta;q)-\varphi_0(\eta)]&=q\hbar_\varphi N_\varphi[\varphi(\eta;q)],\end{aligned} \quad (30)$$

where $\hbar_H$, $\hbar_\theta$, and $\hbar_\varphi$ denote the auxiliary parameters and $q\ \epsilon\ [0,1]$ represents the embedding parameter. And,

$$\begin{aligned}N_H[H(\eta;q)]&=\frac{\partial^4H(\eta,q)}{\partial\eta^4}-RH(\eta,q)\left(\frac{\partial^3H(\eta,q)}{\partial\eta^3}\right)-R\lambda_1\left(H(\eta,q)\left(\frac{\partial H(\eta,q)}{\partial\eta}\right)\left(\frac{\partial^3H(\eta,q)}{\partial\eta^3}\right)\right.\\&\quad\left.+H^2(\eta,q)\left(\frac{\partial^4H(\eta,q)}{\partial\eta^4}\right)-\left(\frac{\partial H(\eta,q)}{\partial\eta}\right)^2\left(\frac{\partial^2H(\eta,q)}{\partial\eta^2}\right)-H(\eta,q)\left(\frac{\partial^2H(\eta,q)}{\partial\eta^2}\right)^2\right)\\&\quad+\lambda_2\left(-2\left(\frac{\partial^2H(\eta,q)}{\partial\eta^2}\right)\left(\frac{\partial^3H(\eta,q)}{\partial\eta^3}\right)+\left(\frac{\partial H(\eta,q)}{\partial\eta}\right)\left(\frac{\partial^4H(\eta,q)}{\partial\eta^4}\right)+H(\eta,q)\left(\frac{\partial^5H(\eta,q)}{\partial\eta^5}\right)\right)\\&\quad+MR\left[\frac{\partial^2H(\eta,q)}{\partial\eta^2}+\lambda_1\left(\left(\frac{\partial H(\eta,q)}{\partial\eta}\right)\left(\frac{\partial^2H(\eta,q)}{\partial\eta^2}\right)+H(\eta,q)\left(\frac{\partial^3H(\eta,q)}{\partial\eta^3}\right)\right)\right],\\N_\theta[\theta(\eta;q)]&=\frac{\partial^2\theta(\eta,q)}{\partial\eta^2}-\mathrm{RPr}H(\eta,q)\frac{\partial\theta(\eta,q)}{\partial\eta},\\N_\varphi[\varphi(\eta;q)]&=\frac{\partial^2\varphi(\eta,q)}{\partial\eta^2}-RSc\left(K_1\varphi(\eta,q)(1-\varphi(\eta,q))^2+H(\eta,q)\frac{\partial\varphi(\eta,q)}{\partial\eta}\right).\end{aligned} \quad (31)$$

The equations for the m-th deformations of the problem are

$$\begin{aligned}
L_H\left[H_m(\eta)-\chi_m H_{m-1}(\eta)\right] &= \hbar_H R_{1m}(\eta),\\
L_\theta\left[\theta_m(\eta)-\chi_m \theta_{m-1}(\eta)\right] &= \hbar_\theta R_{2m}(\eta),\\
L_\varphi\left[\varphi_m(\eta)-\chi_m \varphi_{m-1}(\eta)\right] &= \hbar_\varphi R_{3m}(\eta),\\
H_m(0) &= H_m(1)=0,\\
H_m'(0) &= \left(\epsilon_1 H_m''(0)+\epsilon_2 H_m'''(0)\right),\quad H_m'(1) = -\left(\epsilon_1 H_m''(1)+\epsilon_2 H_m'''(1)\right),\\
\theta_m(0) &= \left(\epsilon_3\theta_m'(0)+\epsilon_4\theta_m''(0)\right),\\
\theta(1) &= -\left(\epsilon_3\theta_m'(1)+\epsilon_4\theta_m''(1)\right),\\
\varphi_m(0) &= 0,\\
\varphi_m'(1) &= K_2\varphi_m(1),\\
\chi_m &= \begin{cases} 0, & m\le 1,\\ 1, & m>0.\end{cases}
\end{aligned} \tag{32}$$

The series solution is computed iteratively for $m = 1, 2, 3, \ldots$ using MATHEMATICA software.

4. Convergence of Solution

In order to obtain the comfortable accuracy of the homotopic solution, the significance of auxiliary parameters cannot be denied. This task has been completed by preparing three h-curves, organized for velocity, temperature, and concentration profiles for some dignified values of emerging parameters. The admissible values of such parameter guaranteed the convergence of the solution. The convergence of the derived series solution is controlled by auxiliary parameters $\hbar_H$, $\hbar_\theta$, and $\hbar_\varphi$. Therefore, we have sketched the $\hbar$-curves in Figure 1 to determine the admissible values of $\hbar_H$, $\hbar_\theta$, and $\hbar_\varphi$. These figures reveal that the convergence region lies within the domain $-0.8 \le \hbar_H \le -0.2, -1.5 \le \hbar_\theta \le -0.4$, and $-1.4 \le \hbar_\varphi \le -0.7$.

In Table 1, the computations have been performed to illustrate the convergence of the obtained solution for $H''(0)$, $\theta'(0)$, and $\varphi'(0)$ at various approximations. Close observations to the table suggest that accuracy of the solution has been obtained at the 15^{th} order of approximations.

5. Physical Interpretations of Results

In this section, the effects of various arising parameters on radial and vertical velocity components, pressure, temperature, and concentration fields are discussed with relevant physical significances.

5.1. Dimensionless Velocity and Pressure Profiles. Figure 2(a) shows the impact of the Hartmann number M on the velocity vertical component by keeping other parameters fixed. The interface of stronger magnetic force is more valuable to decay the motion of fluid particles. A small increment in velocity was observed first which decreases up to a certain height. Physically, as M increases, the Lorentz force boosts up which resists the flow of liquid due to which velocity decay occurs. Therefore, the presence of magnetic field combats the transport phenomena and subsequently diminishes the vertical velocity. The effects of wall stretching parameter γ on the velocity profile are shown in Figure 2(b). The vertical velocity component rises up with a variation of γ. However, a change in the radial component is not similar to vertical components. Here, velocity increases at a specific range and then gradually decreases. Figure 2(c) delineates the significance of the Deborah number in terms of relaxation time λ_1 on vertical and radial component of velocities. A rise in the vertical component of velocity is observed for larger values of the Deborah number; however, the radial component of velocity decreases smoothly after a small increment. The variation of material parameter λ_2 on both vertical and radial velocity components is illustrated in Figure 2(d). The reverse trend is observed as compared to λ_1 for both components. We observe from Figures 2(e) and 2(f) that when we increase of first- and second-order velocity slip constants (ϵ_1, ϵ_2), the vertical velocity component also increases. Physically, with increase of velocity slip parameters, the stretching velocity affects the movement of fluid so velocity profiles get maximum values. Moreover, the amplitude of radial velocity increases up to a specific range due to the difference of the stretching rate. Figures 2(g) and 2(h) show that the skin friction coefficient increases with increase of both slip parameters. It is scrutinized from Figure 2(i) that pressure decreases in the whole domain by increasing values of the Hartmann number M. It is found from Figure 2(j) that decay in pressure is observed by increasing the velocity slip parameter.

5.2. Dimensionless Temperature Profile. In Figures 3(a) and 3(b), the dimensionless temperature $\theta(\eta)$ is plotted to study the impact of the velocity slip parameter. The temperature decreases by increasing both velocity slip parameters. It is elucidated from Figures 3(c) and 3(d) that the distribution of temperature θ boosts up due to alteration of the first- and

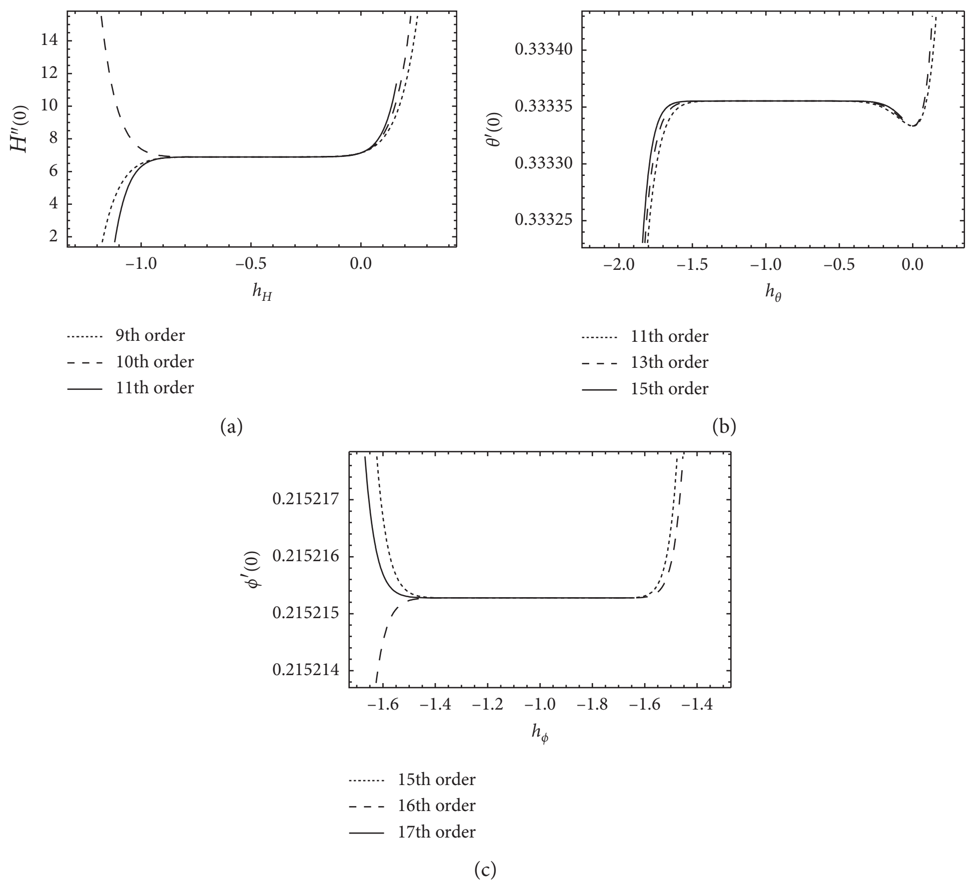

Figure 1: $\hbar$-curves for (a) $\hbar_H$, (b) $\hbar_\theta$, and (c) $\hbar_\varphi$ with $R = 2, \gamma = 0.5, M = 0.3, K_2 = 0.2, \mathrm{Pr} = 0.5, \lambda_1 = \lambda_2 = 0.2, K_1 = 0.5, Sc = 0.2, \epsilon_1 = 0.2, \epsilon_2 = 0.3, \epsilon_3 = 0.3$, and $\epsilon_4 = 0.5$..

Table 1: The HAM convergence at different order of approximations.

Approximation	$H''(0)$	$\theta'(0)$	$\varphi'(0)$
07	6.89132	0.499908	0.214794
10	6.89123	0.499907	0.215223
13	6.89122	0.499906	0.215228
14	6.89121	0.499905	0.215215
15	6.89120	0.499905	0.215215

second-order temperature jump parameters. Physically, due to slip effect, more flow penetrates through the thermal boundary with an increase in temperature jump parameters. Figure 3(e) accomplishes the significance of the Prandtl number Pr on the temperature profile. The impression Pr declined the temperature of the fluid effectively. The dimensionless number Pr depends upon thermal diffusivity which decreases by increasing Pr. Therefore, a decline in the temperature field is observed. Thus, higher values of Pr correspond to lower thermal diffusivity and subsequently declining temperature distribution. Figure 3(f) exhibits the dominant effect of the Hartmann number M on the temperature profile. As expected, the temperature of fluid increases by increasing M. Physically, the applied magnetic field produces the Lorentz force, which creates a drag force which has a tendency to enhance the temperature of the fluid between both disks.

5.3. Dimensionless Concentration Profile. Taking into account of the concentration profile φ, the effects for various parameters are encountered. First, we consider the variation of the homogeneous reaction K_1 on φ. An increase in K_1 results in diminishing of the concentration profile (Figure 4(a)). Figure 4(b) shows the consequence of heterogeneous reaction parameter K_2 on the concentration profile. The rate of mass transfer is enhanced by increasing K_2. Figure 4(c) shows that the rate of mass transfer solely decreases by varying Schmidt number Sc. Sc has an inverse relation with molecular diffusivity which decreases by increasing Sc. The variation of different values of the strengths of the homogeneous parameter K_1 and heterogeneous reaction parameter K_2 on wall concentration on both disks is shown in Figures 5 and 6, respectively. These figures indicate that values of $\varphi'(0)$ and $\varphi'(1)$ increase by increasing K_1 while contradictory behavior is noted for K_2.

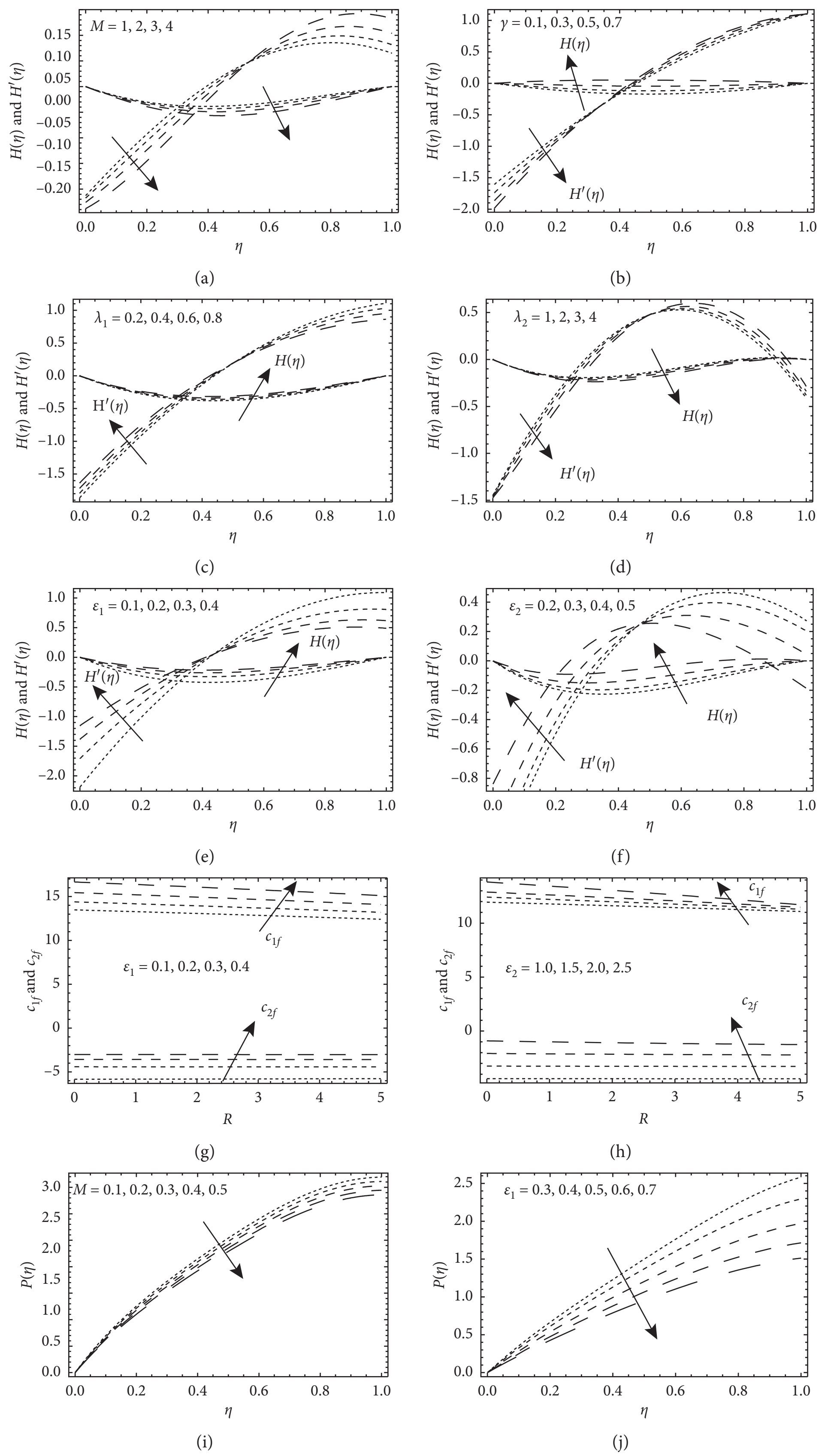

Figure 2: (a)–(f) Graphs of vertical and radial components of velocity, (g)-(h) graphs of for skin friction, and (i)-(j) graphs of pressure for different values of $\gamma = 0.5, \hbar_H = -0.5, \hbar_\theta = -1.2, \hbar_\varphi = -1.0, M = 0.3, R = 5, \epsilon_1 = 0.5, \epsilon_2 = 0.2, \lambda_1 = 0.2$, and $\lambda_2 = 0.5$. (a) Effects of the Hartmann number, (b) effects of the stretching parameter, (c) effects of the Deborah number of relaxation, (d) effects of the Deborah number of retardation, (e) effects of the first-order velocity slip parameter, (f) effects of the second-order velocity slip parameter, (g) influence of the first-order velocity slip parameter on the skin friction coefficient, (h) influence of the second-order velocity slip parameter on the skin friction coefficient, (i) Influence of Hartmann number on pressure (j) Influence of first-order velocity slip parameter on pressure.

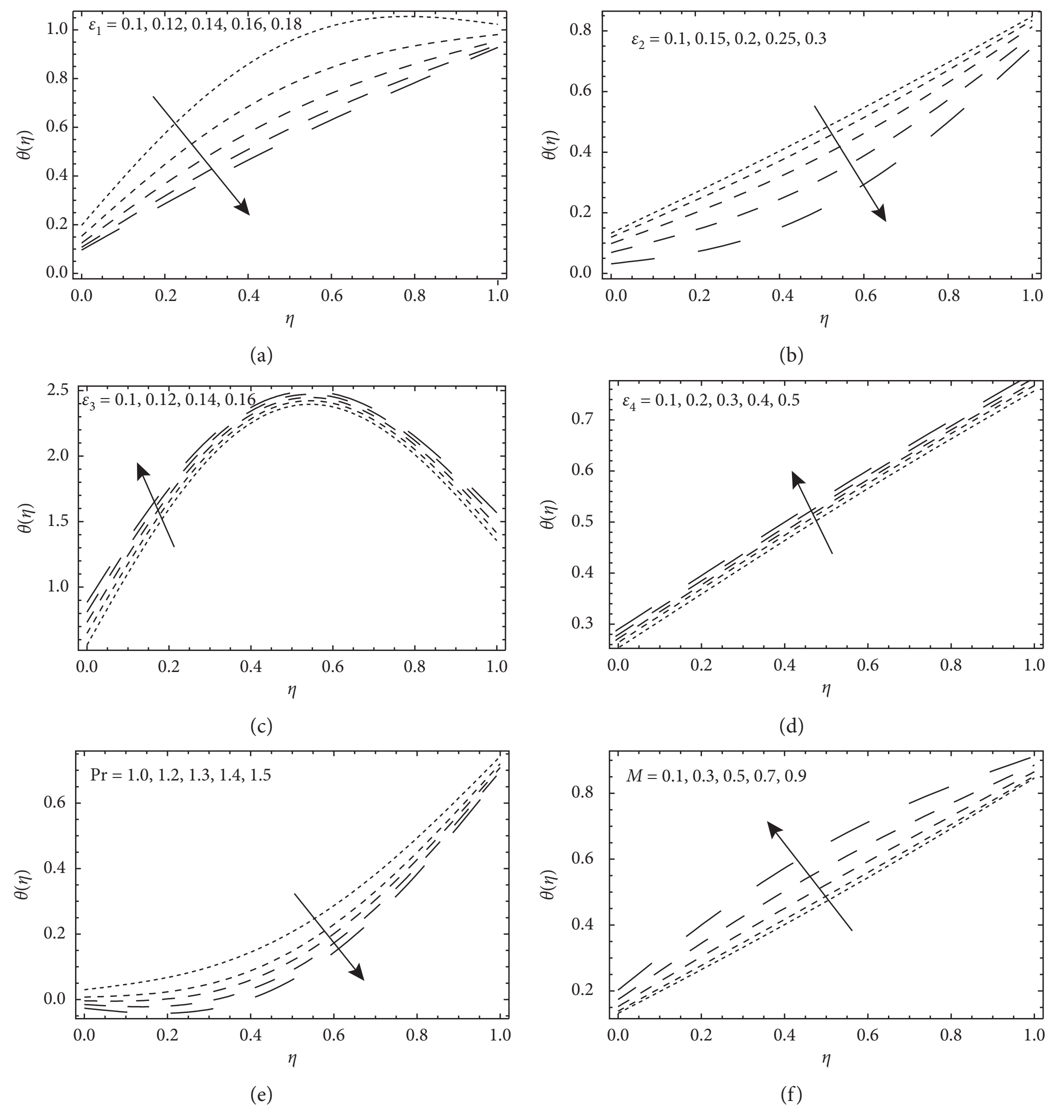

Figure 3: Temperature profile with $\gamma = 0.5, \hbar_H = -0.5, \hbar_\theta = -1.2, \hbar_\varphi = -1.0, M = 0.3, R = 5, \epsilon_1 = \epsilon_2 = 0.2, \epsilon_3 = 0.3, \epsilon_4 = 0.5, \lambda_1 = 0.2$, and $\lambda_2 = 0.5$. (a) Influence of the first-order velocity slip parameter, (b) influence of the second-order velocity slip parameter, (c) variation of the first-order temperature jump parameter, (d) variation of the second-order temperature jump parameter, (e) variation of the Hartmann number, and (f) variation of the Prandtl number.

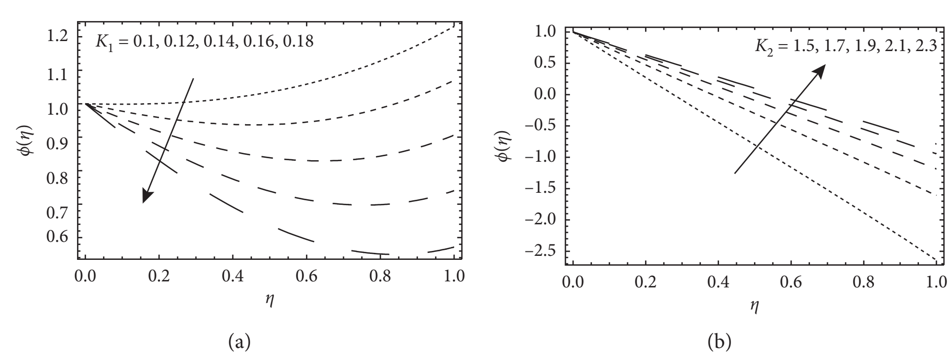

Figure 4: Continued.

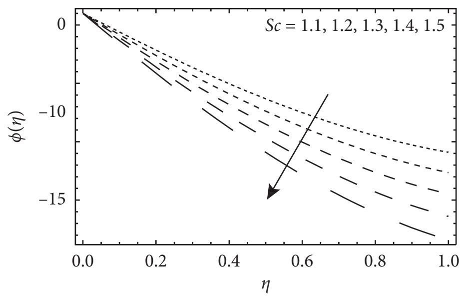

(c)

Figure 4: Concentration distribution for $\gamma = 0.5, \hbar_H = -0.5, \hbar_\theta = -1.2, \hbar_\varphi = -1.0, M = 0.3, R = 2, \epsilon_1 = \epsilon_2 = 0.2, \epsilon_3 = 0.3, \epsilon_4 = 0.5, \lambda_1 = 0.2$, and $\lambda_2 = 0.2$. (a) Influence of strength of the homogeneous reaction, (b) influence of strength of the heterogeneous reaction, and (c) influence of strength of the Schmidt number.

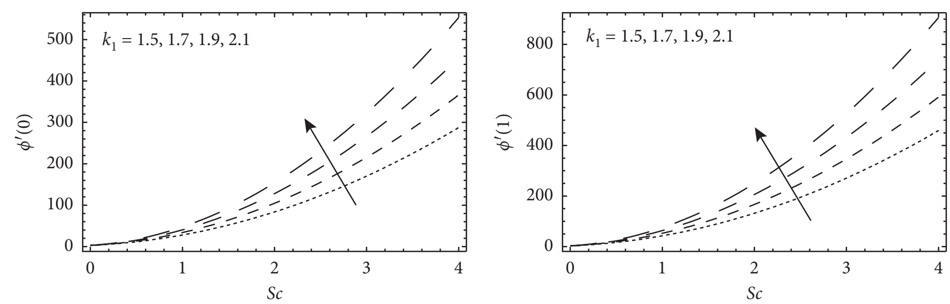

(a) (b)

Figure 5: Influence of strength of the homogeneous reaction.

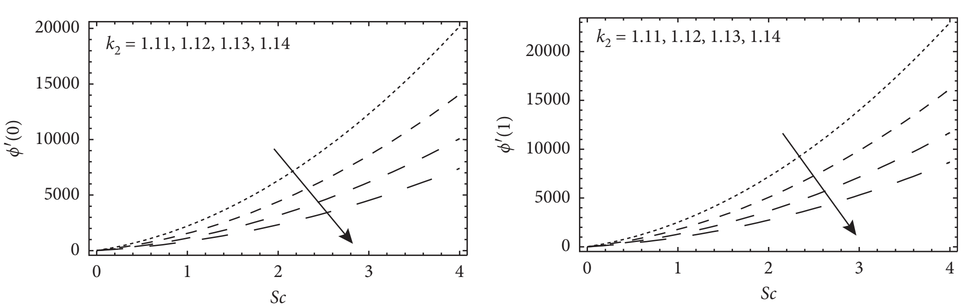

(a) (b)

Figure 6: Influence of strength of the heterogeneous reaction.

5.4. Local Nusselt Number. Table 2 aims to elaborate the iterative numerical variation in the local Nusselt number against involved fluid parameters. We found that with the increase in the velocity slip parameter, the temperature profile at the lower disk increases. The heat transfer rate decreases by increasing the Hartmann number M at the lower disk. However, opposite values for M are observed for the upper disk. Such observations are made as both disks are stretched with different velocities.

6. Conclusions

In this work, a chemically reactive flow of Oldroyd-B fluid subject to stretchable disks is considered in presence of homogeneous and heterogeneous chemical reactions. The homogeneous-heterogeneous reactions are considered in the concentration equation. The physical features are visualized for various involved parameters graphically. The important observations are summarized as follows:

Table 2: Variation in the local Nusselt number at lower and upper disks.

ϵ_1	ϵ_2	ϵ_3	ϵ_4	Pr	M	Lower disk	Upper disk
0.1	0.5	0.5	0.2	1.0	0.3	−0.66799	−0.75961
0.2	0.5	0.5	0.2	1.0	0.3	−0.65734	−0.73076
0.3	0.5	0.5	0.2	1.0	0.3	−0.64662	−0.72170
0.2	0.1	0.5	0.2	1.0	0.3	−0.66799	−0.75961
0.2	0.2	0.5	0.2	1.0	0.3	−0.50683	−0.61961
0.2	0.3	0.5	0.2	1.0	0.3	−0.17056	−0.25760
0.2	0.5	0.1	0.2	1.0	0.3	−0.70753	−0.66151
0.2	0.5	0.2	0.2	1.0	0.3	−0.89202	−0.73829
0.2	0.5	0.3	0.2	1.0	0.3	−0.90542	−0.84591
0.2	0.5	0.5	1.0	1.0	0.3	−0.52624	−0.46733
0.2	0.5	0.5	2.0	1.0	0.3	−0.52626	−0.46736
0.2	0.5	0.5	3.0	1.0	0.3	−0.52628	−0.46739
0.2	0.5	0.5	0.2	0.1	0.3	−0.49842	−0.50166
0.2	0.5	0.5	0.2	0.2	0.3	−0.49684	−0.50332
0.2	0.5	0.5	0.2	0.3	0.3	−0.49527	−0.50498
0.2	0.5	0.5	0.2	1.0	0.1	−0.46169	−0.53829
0.2	0.5	0.5	0.2	1.0	0.2	−0.46974	−0.53052
0.2	0.5	0.5	0.2	1.0	0.3	−0.48423	−0.51662

(i) The velocity distribution increases with variation of slip parameters while it decreases with the Deborah number for retardation time.

(ii) The concentration distribution declines with increment of the Schmidt number and the homogeneous reaction while effects of the heterogeneous reaction parameter are quite reverse.

(iii) The temperature distribution increases by increasing the Hartmann number while lower temperature distribution is observed for larger values of the Prandtl number.

(iv) The presence of first- and second-order velocity slip results in an increment in the wall shear stress.

Data Availability

No data were used to support this study.

Conflicts of Interest

The authors declare no conflicts of interest.

References

[1] L. Zheng, C. Zhang, X. Zhang, and J. Zhang, "Flow and radiation heat transfer of a nanofluid over a stretching sheet with velocity slip and temperature jump in porous medium," *Journal of the Franklin Institute*, vol. 350, no. 5, pp. 990–1007, 2013.

[2] K. Vajravelu, S. Sreenadh, and R. Saravana, "Combined influence of velocity slip, temperature and concentration jump conditions on MHD peristaltic transport of a Carreau fluid in a non-uniform channel," *Applied Mathematics and Computation*, vol. 225, pp. 656–676, 2013.

[3] W. A. Khan, J. Uddin, and A. L. Ismail, "Hydrodynamic and thermal slip effect on double-diffusive free convective boundary layer flow of a nanofluid past a flat vertical plate in the moving free stream," *PLoS One*, vol. 8, no. 3, Article ID e54024, 2013.

[4] N. Xiao, J. Elsnab, and T. Ameel, "Microtube gas flows with second-order slip flow and temperature jump boundary conditions," *International Journal of Thermal Sciences*, vol. 48, no. 2, pp. 243–251, 2009.

[5] S. A. Rooholghdos and E. Roohi, "Extension of a second order velocity slip/temperature jump boundary condition to simulate high speed micro/nanoflows," *Computers & Mathematics with Applications*, vol. 67, no. 11, pp. 2029–2040, 2014.

[6] N. T. P. Le and E. Roohi, "A new form of the second-order temperature jump boundary condition for the low-speed nanoscale and hypersonic rarefied gas flow simulations," *International Journal of Thermal Sciences*, vol. 98, pp. 51–59, 2015.

[7] A. Sinha, G. C. Shit, and N. K. Ranjit, "Peristaltic transport of MHD flow and heat transfer in an asymmetric channel: effects of variable viscosity, velocity-slip and temperature jump," *Alexandria Engineering Journal*, vol. 54, no. 3, pp. 691–704, 2015.

[8] M. A. El-Aziz and A. A. Afify, "Influences of slip velocity and induced magnetic field on MHD stagnation-point flow and heat transfer of Casson fluid over a stretching sheet," *Mathematical Problems in Engineering*, vol. 2018, Article ID 9402836, 11 pages, 2018.

[9] Z. Khan, H. U. Rasheed, S. Noor et al., "Analytical solution of UCM viscoelastic liquid with slip condition and heat flux over stretching sheet: the Galerkin approach," *Mathematical Problems in Engineering*, vol. 2020, Article ID 7563693, 7 pages, 2020.

[10] R. Muhammad, M. I. Khan, N. B. Khan, and M. Jameel, "Magnetohydrodynamics (MHD) radiated nanomaterial viscous material flow by a curved surface with second order slip and entropy generation," *Computer Methods and Programs in Biomedicine*, vol. 189, Article ID 105294, 2020.

[11] S. Aman, Q. Al-Mdallal, and I. Khan, "Heat transfer and second order slip effect on MHD flow of fractional Maxwell fluid in a porous medium," *Journal of King Saud University-Science*, vol. 32, no. 1, pp. 450–458, 2020.

[12] T. V. Kármán and T. Uber, "Über laminare und turbulente Reibung," *ZAMM—Journal of Applied Mathematics and Mechanics/Zeitschrift für Angewandte Mathematik und Mechanik*, vol. 1, no. 4, pp. 233–252, 1921.

[13] T. Hayat, A. Shafiq, M. Nawaz, and A. Alsaedi, "MHD axisymmetric flow of third grade fluid between porous disks with heat transfer," *Applied Mathematics and Mechanics*, vol. 33, no. 6, pp. 749–764, 2012.

[14] M. Turkyilmazoglu, "Three dimensional MHD stagnation flow due to a stretchable rotating disk," *International Journal of Heat and Mass Transfer*, vol. 55, no. 23-24, pp. 6959–6965, 2012.

[15] M. Turkyilmazoglu, "MHD fluid flow and heat transfer due to a shrinking rotating disk," *Computers & Fluids*, vol. 90, pp. 51–56, 2014.

[16] S. K. Soid, A. Ishak, and I. Pop, "MHD flow and heat transfer over a radially stretching/shrinking disk," *Chinese Journal of Physics*, vol. 56, no. 1, pp. 58–66, 2018.

[17] C. Yin, L. Zheng, C. Zhang, and X. Zhang, "Flow and heat transfer of nanofluids over a rotating disk with uniform stretching rate in the radial direction," *Propulsion and Power Research*, vol. 6, no. 1, pp. 25–30, 2017.

[18] M. Turkyilmazoglu, "Fluid flow and heat transfer over a rotating and vertically moving disk," *Physics of Fluids*, vol. 30, no. 6, Article ID 063605, 2018.

[19] M. S. Hashmi, N. Khan, S. Ullah Khan, and M. M. Rashidi, "A Mathematical model for mixed convective flow of chemically reactive Oldroyd-B fluid between isothermal stretching disks," *Results in Physics*, vol. 7, pp. 3016–3023, 2017.

[20] J. Li, L. Zheng, and L. Liu, "MHD viscoelastic flow and heat transfer over a vertical stretching sheet with Cattaneo-Christov heat flux effects," *Journal of Molecular Liquids*, vol. 221, pp. 19–25, 2016.

[21] A. Ghaffari, T. Javed, and K.-L. Hsiao, "Heat transfer analysis of unsteady oblique stagnation point flow of elastico-viscous fluid due to sinusoidal wall temperature over an oscillating-stretching surface: a numerical approach," *Journal of Molecular Liquids*, vol. 219, pp. 748–755, 2016.

[22] Z. Tadmor and I. Klein, "Engineering principles of plasticating extrusion," in *Polymer Science and Engineering Series*, Van Norstrand Reinhold, New York, NY, USA, 1970.

[23] N. Ali, S. U. Khan, Z. Abbas, and M. Sajid, "Flow and heat transfer of MHD oldroyd-B fluid in a channel with stretching walls," *Nonlinear Engineering*, vol. 5, no. 2, pp. 73–79, 2016.

[24] B. C. Sakiadis, "Boundary-layer behavior on continuous solid surfaces: I. Boundary-layer equations for two-dimensional and axisymmetric flow," *AIChE Journal*, vol. 7, no. 1, pp. 26–28, 1961.

[25] B. C. Sakiadis, "Boundary-layer behavior on continuous solid surfaces: II. The boundary layer on a continuous flat surface," *AIChE Journal*, vol. 7, no. 2, pp. 221–225, 1961.

[26] C. Y. Wang, "Exact solutions of the steady-state Navier-Stokes equations," *Annual Review of Fluid Mechanics*, vol. 23, no. 1, pp. 159–177, 1991.

[27] T. Fang, "Flow over a stretchable disk," *Physics of Fluids*, vol. 19, no. 12, p. 128105, 2007.

[28] T. Fang and J. Zhang, "Flow between two stretchable disks-an exact solution of the Navier-Stokes equations," *International Communications in Heat and Mass Transfer*, vol. 35, no. 8, pp. 892–895, 2008.

[29] R. A. V. Gorder, E. Sweet, and K. Vajravelu, "Analytical solutions of a coupled nonlinear system arising in a flow between stretching disks," *Applied Mathematics and Computation*, vol. 216, no. 5, pp. 1513–1523, 2010.

[30] S. T. Mohyud-Din and S. I. Khan, "Nonlinear radiation effects on squeezing flow of a Casson fluid between parallel disks," *Aerospace Science and Technology*, vol. 48, pp. 186–192, 2016.

[31] M. M. Rashidi, T. Hayat, E. Erfani, S. A. Mohimanian Pour, and A. A. Hendi, "Simultaneous effects of partial slip and thermal-diffusion and diffusion-thermo on steady MHD convective flow due to a rotating disk," *Communications in Nonlinear Science and Numerical Simulation*, vol. 16, no. 11, pp. 4303–4317, 2011.

[32] N. Khan, M. Sajid, and T. Mahmood, "Flow of a hydromagnetic viscous fluid between parallel disks with slip," *Journal of Mechanics*, vol. 31, no. 6, pp. 713–726, 2015.

[33] N. Khan, M. Sajid, and T. Mahmood, "Heat transfer analysis for magnetohydrodynamics axi-symmetric flow between stretching disks in the presence of viscous dissipation and joule heating," *AIP Advances*, vol. 5, Article ID 057115, 2015.

[34] S. A. Khan, T. Saeed, M. Ijaz Khan, T. Hayat, M. I. Khan, and A. Alsaedi, "Entropy optimized CNTs based Darcy-Forchheimer nanomaterial flow between two stretchable rotating disks," *International Journal of Hydrogen Energy*, vol. 44, no. 59, pp. 31579–31592, 2019.

[35] D.-H. Doh, G.-R. Cho, and M. Muthtamilselvan, "Cattaneo-Christov heat flux model for inclined MHD micropolar fluid flow past a non-linearly stretchable rotating disk," *Case Studies in Thermal Engineering*, vol. 14, p. 100496, 2019.

[36] A. Renuka, M. Muthtamilselvan, D.-H. Doh, and G.-R. Cho, "Entropy analysis and nanofluid past a double stretchable spinning disk using Homotopy Analysis Method," *Mathematics and Computers in Simulation*, vol. 171, pp. 152–169, 2020.

[37] J. H. Merkin, "A model for isothermal homogeneous-heterogeneous reactions in boundary-layer flow," *Mathematical and Computer Modelling*, vol. 24, no. 8, pp. 125–136, 1996.

[38] P. K. Kameswaran, S. Shaw, P. Sibanda, and P. V. S. N. Murthy, "Homogeneous-Heterogeneous reactions in a nanofluid flow due to a porous stretching sheet," *International Journal of Heat and Mass Transfer*, vol. 57, no. 2, pp. 465–472, 2013.

[39] T. Hayat, M. Imtiaz, and A. Alsaedi, "Impact of magnetohydrodynamics in bidirectional flow of nanofluid subject to second order slip velocity and homogeneous-heterogeneous reactions," *Journal of Magnetism and Magnetic Materials*, vol. 395, pp. 294–302, 2015.

[40] S. J. Liao, *Beyond Perturbation: Introduction to the Homotopy Analysis Method*, Chapman & Hall, Boca Raton, MA, USA, 2003.

[41] S.-J. Liao, "On the analytic solution of magnetohydrodynamic flows of non-Newtonian fluids over a stretching sheet," *Journal of Fluid Mechanics*, vol. 488, pp. 189–212, 2003.

[42] M. Turkyilmazoglu, "Solution of the Thomas-Fermi equation with a convergent approach," *Communications in Nonlinear Science and Numerical Simulation*, vol. 17, no. 11, pp. 4097–4103, 2012.

[43] M. Turkyilmazoglu, "Parametrized Adomian decomposition method with optimum convergence," *ACM Transactions on Modeling and Computer Simulation*, vol. 27, no. 4, pp. 1–21, 2017.

[44] S. U. Khan, N. Ali, and T. Hayat, "Analytical and numerical study of diffusion of chemically reactive species in eyring-powell fluid over an oscillatory stretching surface," *Bulgarian Chemical Communications*, vol. 49, no. 2, pp. 320–330, 2017.

[45] S. Ullah Khan, A. Rauf, S. Ali Shehzad, Z. Abbas, and T. Javed, "Study of bioconvection flow in oldroyd-B nanofluid with motile organisms and effective Prandtl approach," *Physica A: Statistical Mechanics and Its Applications*, vol. 527, Article ID 121179, 2019.

[46] J. H. Merkin and M. A. Chaudhary, "A simple isothermal model for homogeneous-heterogeneous reactions in boundary layer flow: I equal diffusivities," *Fluid Dynamics Research*, vol. 16, no. 6, pp. 311–333, 1995.